ELASTICITY-BASED TISSUE CHARACTERIZATION OF ARTERIAL WALL

HIDEYUKI HASEGAWA[1)2)], KENTARO TSUZUKI[2)], MASATAKA ICHIKI[3)],
FUMIAKI TEZUKA[4)], HIROSHI KANAI[2)1)]

1) Graduate School of Biomedical Engineering, Tohoku University,
6-6-05 Aramaki-aza-Aoba, Aoba-ku, Sendai 980-8579, Japan

2) Graduate School of Engineering, Tohoku University,
6-6-05 Aramaki-aza-Aoba, Aoba-ku, Sendai 980-8579, Japan

3) Sendai Hospital of East Railway Company,   *1-*
1-5 Itsutsubashi, Aoba-ku, Sendai 980-8508, Japan

4) Sendai Medical Center, 2-8-8 Miyagino, Miyagino-ku, Sendai 983-8520, Japan

Pathological changes in arterial walls significantly influence their mechanical properties. We have developed a correlation-based method, the *phased-tracking method*, for measurement of the regional elasticity of the arterial wall. Using this method, elasticity distributions of lipids, blood clots, fibrous tissue, and calcified tissue were measured by *in vitro* experiments of excised arteries (mean $\pm$ SD: lipid, 89 $\pm$ 47 kPa; blood clot, 131 $\pm$ 56 kPa; fibrous tissue, 1022 $\pm$ 1040 kPa; calcified tissue, 2267 $\pm$ 1228 kPa). It was found that arterial tissues can be classified into soft tissues (lipids and blood clots) and hard tissues (fibrous tissue and calcified tissue) on the basis of their elasticity. However, there are large overlaps between elasticity distributions of lipids and blood clots and those of fibrous tissue and calcified tissue. Thus, it was difficult to differentiate lipids from blood clots and fibrous tissue from calcified tissue when a threshold for a single elasticity value was set. Therefore, we developed and optimized a tissue classification method using the elasticity distribution in each small region. In this method, the elasticity distribution of each small region of interest (ROI) (not a single pixel) in an elasticity image is used to classify lipids, blood clots, fibrous tissue, and calcified tissue by calculating the likelihood function for each tissue. The ratio of correctly classified pixels to the total number of classified pixels was 29.8% when the size of a small region was 75 μm × 300 μm (a single pixel), but became 54.2% when the size of a small region was 1,500 μm × 1,500 μm (100 pixels).

1. Introduction

Noninvasive measurement of elasticity of the arterial wall is useful for diagnosis of atherosclerosis because there are significant differences between

1

 the elasticity of a normal arterial wall and that of an arterial wall affected by atherosclerosis [1]. In particular, mechanical properties of atherosclerotic plaque are important because plaque rupture may cause acute myocardial infarction and cerebral infarction [2-4]. Magnetic resonance imaging (MRI) and intravascular ultrasound (IVUS) are promising technologies for directly imaging plaque morphology [5,6]. On the other hand, the dynamic change of artery diameter due to the pulsation of the heart can be measured noninvasively by conventional methods with ultrasound [7-10]. Some parameters related to artery-wall elasticity can be obtained by the measured change in diameter of the artery [11-13]. However, in the derivation of these parameters, the artery is assumed to be a cylindrical shell with an uniform wall thickness and, thus, the elasticity of atherosclerotic plaque cannot be evaluated.

For measurement of the mechanical properties of the arterial wall, including the case with atherosclerotic plaque, we previously developed a method, namely, the *phased-tracking method*, for measuring small vibrations in the heart wall or arterial wall with transcutaneous ultrasound [14]. For a number of years, we have been measuring the displacement and small change in thickness of the arterial wall caused by the heartbeat using this method for elasticity imaging [15-17]. Elasticity images of the human carotid artery have been obtained by the measured distribution of changes in thickness, and the potential for transcutaneous tissue characterization has been shown by classifying the elasticity images using elasticity reference data obtained by *in vitro* experiments [16,18,19].

We have already measured the elasticity distributions for lipids, blood clots, fibrous tissue (mixture of the smooth muscle and collagen), and calcified tissue. In these previous studies, it was found that arterial tissues can be classified into soft tissues (lipids, blood clots) and hard tissues (fibrous tissue, calcified tissue) on the basis of their elasticity. However, it was difficult to differentiate lipids from blood clots and fibrous tissue from calcified tissue. We thus proposed a tissue classification method using the elasticity distribution in a small region [20]. In this method, the elasticity distribution of each small ROI (not a single pixel) in an elasticity image was used to classify lipids, blood clots, fibrous tissue, and calcified tissue. The precision of tissue classification was improved using the elasticity distribution in each small region.

However, the accuracy of this method in relation to the size of an ROI has not yet been thoroughly investigated. In the present study, to determine the optimum size of an ROI, the accuracy of tissue classification (including calcified tissue) was quantitatively investigated in relation to the size of the ROI.

In addition, in the proposed classification method, an ROI is classified into one of the four tissue components, *i.e.* lipids, blood clots, fibrous tissue, and calcified tissue, even when the maximum likelihood is low. In the present study, such a region is defined as an unclassified region by setting a threshold for the likelihood. From these investigations, tissue classification was much improved in comparison with that in the previous study [21,22].

2. Materials and Methods

2.1. *Experimental setup and specimens*

Change in the pressure inside an excised artery was realized by circulating a fluid using a flow pump. The fluid inside the artery and that circulating in the flow pump were separated by a rubber membrane to prevent the flow pump from being contaminated, and only the change in internal pressure propagated to the inside of the artery. The change in internal pressure was measured by a pressure transducer (Model 110-4, Camino, San Diego, CA, USA).

In the acquisition of ultrasonic echoes, excised arteries (eight iliac and ten femoral) were measured with a conventional 7.5 MHz linear-type ultrasonic probe (SSH-140A, Toshiba, Japan). The quadrature demodulated signals of RF echoes were acquired at 10 MHz at a frame rate of 200 Hz. The elasticity of the arterial wall was defined as the tissue strain calibrated by the average stress of the entire wall thickness, namely, the circumferential elastic modulus E_θ^h [17]. The strain distribution was obtained by applying the *phased-tracking method* to the measured demodulated signals [17]. During the ultrasonic measurement, a needle was attached to the external surface of the artery for identification of the measured section so that a pathological image of the same section could be obtained after the ultrasonic measurement.

2.2. *Tissue classification using the likelihood function*

Each pixel in an elasticity image was classified into one of 5 categories, namely, lipids, blood clots, fibrous tissue, calcified tissue, and unknown using the likelihood function $\{L_i\}$ (i = 1: lipid; 2: blood clot; 3: fibrous tissue; 4: calcified tissue) of the elasticity distribution in the small region around the pixel. To obtain the likelihood function $\{L_i\}$, the elasticity distribution of the i-th tissue was translated into the normal distribution to describe the probability distribution by the mean and the standard deviation as described below [20].

From *in vitro* experiments, the elasticity distribution of each tissue i was obtained as illustrated in Fig. 1(a). The elasticity distribution of the i-th tissue

consists of J_i data points with the respective elastic moduli. Using all data of J_i points (J_1: 228, J_2: 179, J_3: 19,121, J_4: 1,101) with the respective elastic moduli, the ascending sequence is constructed for tissue i as shown in Fig. 1(b). In this sequence, the j-th datum ($j = 1, 2, . . ., J_i$) has the corresponding elastic modulus E_j ($E_j \leq E_{j+1}$), where j was termed the elasticity number. The probability distribution of each tissue was obtained by allocating all the data of J_i points of each tissue i to boxes of the normal distribution. The box numbers, $\{B_i\}$, of the normal distribution are determined so that the number of data in the box at each end is only one. As shown in Fig. 1(c), the number of data, $D_{i,h}$ ($h = 1, 2, . . ., B_i$), included in box B_i is determined so as to follow the profile of the normal distribution. Thus, the (J_i / 2)-th datum is included in the box with the highest probability. By allocating all the data of J_i points of each tissue to boxes of the corresponding normal distribution, the mean elasticity $\bar{E}_{i,h}$ of the data included in each box was obtained.

ROIs were assigned to an elasticity image which was obtained by ultrasonic measurement. The likelihood function $L_i(m,n)$ is defined as the joint probability that all the elasticity values in ROI $R_{m,n}$ (center of ROI: n-th sampled point along the m-th beam) simultaneously belong in the i-th category as follows:

$$L_i(m,n) = \left(\prod_{(k,l) \in R_{m,n}} p_i(E_{k,l}) \right)^{1/N_0} \quad (i = 1, 2, 3, 4), \tag{2.1}$$

where $p_i(E_{k,l})$ is the probability density which shows the probability that elasticity value $E_{k,l}$ in the k-th row and l-th column in an ROI belongs to the i-th tissue category, and N_0 denotes the number of pixels in an ROI $R_{m,n}$. The multiplier $1/N_0$ shows the geometric mean for compensation of the effect of the size of an ROI. The pixel at the center of an ROI is classified into the class which has the maximum likelihood.

In this classification, there may be a region which has an extremely small value for the maximum likelihood. Such regions are classified as unclassified regions by setting threshold T_o to the maximum likelihood. Thus, the category $C(R_{m,n})$, to which an ROI $R_{m,n}$ belongs, is expressed as follows:

$$C(R_{m,n}) = \begin{cases} \arg \max_{1 \leq i \leq 4} L_i(m,n) \\ \quad (\text{if } \max_{1 \leq i \leq 4} L_i(m,n) \geq T_o) . \\ \text{unknown} \qquad (\text{otherwise}) . \end{cases} \tag{2.2}$$
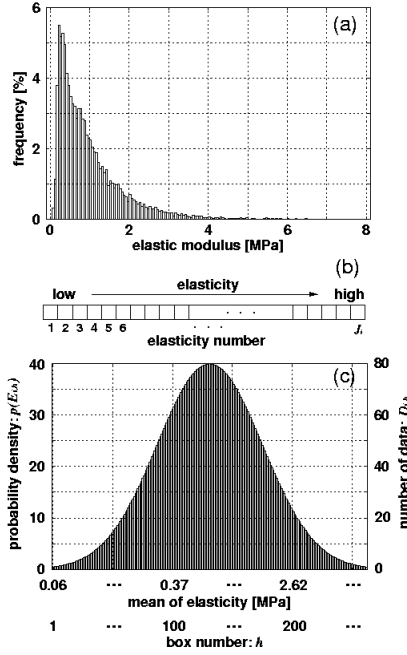
Figure 1. (a) Original elasticity distribution of the tissue. (b) Ascending sequence of the elastic modulus in an elasticity distribution. (c) Normal distribution whose number of boxes depends on the number of data points of (a).

By comparing the pathology-based classification images with the tissue classification images obtained by the proposed method, the recognition rate $R_r(S_{ROI})$ for all tissues in the arterial wall was defined as the ratio of the number of correctly classified pixels to the number N of all pixels in the image as follows:

$$R_r(S_{ROI}) = \frac{\sum_i N_i}{N} \times 100 \ [\%],$$

(2.3)

where N_i is the number of correctly classified pixels of tissue i and S_{ROI} is the size of an ROI. Recognition rate $R_r(S_{ROI})$ was used to determine the optimum size of an ROI.

For an ROI with a very low likelihood for all classes (i = 1, 2, 3, 4), the pixel which is located at the center of the ROI should be defined as an unclassified pixel by thresholding. For determination of the optimum threshold

for the likelihood function, the false recognition rate $F_r(S_{ROI})$ for all tissues in the arterial wall was defined as the ratio of the number of misclassified pixels, except for the pixels classified as unclassified pixels, to the number N of all pixels as follows:

$$F_r(S_{ROI}) = \frac{\sum_i F_i}{N} \times 100 \; [\%],$$

(2.4)

where F_i is the number of misclassified pixels of tissue i, except for the pixels classified as unclassified pixels. Although the unclassified pixels are included in the denominator of eqs. (2.3) and (2.4), that is, the number of all pixels N, they are not included in the number of correctly classified pixels N_i nor that of misclassified pixels F_i. Therefore, the sum of the recognition rate $R_r(S_{ROI})$ and the false recognition rate $F_r(S_{ROI})$ does not become 100%.

3. *In Vitro* Experimental Results

3.1. *Measurement of elasticity distribution of each tissue*

Figure 2 shows the elasticity distribution of each tissue, that is, the frequency of the elasticity values which belong to the range defined by the position and width of each vertical bar. The width of a vertical bar was set at 50 kPa. Means and standard deviations are 89 ± 47 (lipids), 131 ± 56 (blood clots), $1{,}022 \pm 1{,}040$ (fibrous tissue), and $2{,}267 \pm 1{,}228$ kPa (calcified tissue). Although similarities were found in the elasticity distributions of lipids and blood clots and in those of fibrous and calcified tissues, differences in the elasticity distributions of these tissues were also found.
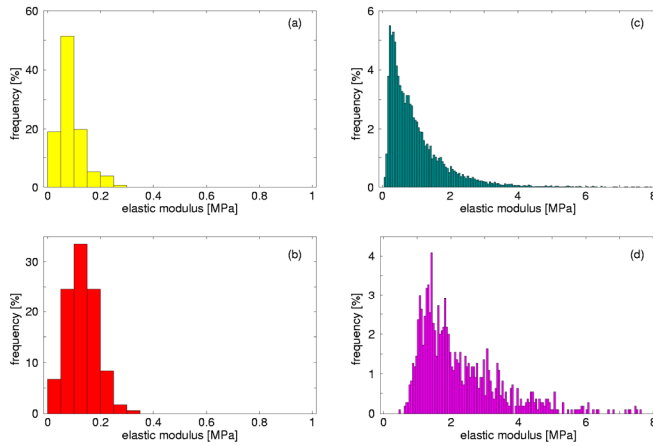
Figure 2. Elasticity distribution of each tissue. (a) Lipids ($N = 288$), (b) blood clots ($N = 178$), (c) fibrous tissue ($N = 19,120$), and (d) calcified tissue ($N = 1,101$).

3.2. *Results of classification*

Figures 3(c) and 3(d) show an example of tissue classification results obtained by the proposed method for an iliac artery. The regions classified as lipids, blood clots, fibrous tissue, and calcified tissue were stained yellow, red, blue, and purple, respectively. Figure 3(c) graphically shows the tissue classification image obtained with an ROI size of 1×1 pixel. Although arterial tissues were roughly classified as soft tissues (lipids and blood clots) and hard tissues (fibrous tissue and calcified tissue), the classified tissue distributions are scattered, and the misclassified regions are prominent. Alternatively, Fig. 3(d) shows the result of classification with an ROI size of 1,500 μm (= 20 pixels) in the radial direction and 1,500 μm (= 5 pixels) in the longitudinal direction. Moreover, the region with low likelihood for all tissue components is colored gray. The threshold T_o for the maximum of the likelihood functions $\{L_i\}$ was set at 0.21. As shown in Fig. 3(d), the region with the maximum likelihood which is higher than threshold T_o is accurately classified as the corresponding tissue identified by referring to the pathological image.

Figure 4 shows the relationship between the size S_{ROI} of an ROI and the recognition rate $R_r(S_{\mathrm{ROI}})$. The ROI size S_{ROI} was changed with its square shape being maintained. The horizontal axis shows the width $W = (S_{\mathrm{ROI}})^{-1/2}$ of an ROI in the longitudinal direction. An ROI consists of a single pixel when width W in Fig. 4 is 0.3 mm. Only in this specific case is an ROI not square (75 μm × 300 μm).

Figure 4(b) shows the relationship between width $W = (S_{\mathrm{ROI}})^{-1/2}$ of an ROI in the longitudinal direction and the recognition rate $R_r(S_{\mathrm{ROI}})$ in arteries which are composed of a single type of tissue, such as fibrous tissue. In such case, the recognition rate $R_r(S_{\mathrm{ROI}})$ is monotonically improved by increasing the size of an ROI because an elasticity image is uniformly classified as the corresponding tissue using a large ROI, which results from the worsening spatial resolution in tissue classification. Figure 4(a) shows the relationship between width W of an ROI and the recognition rate $R_r(S_{\mathrm{ROI}})$ in arteries composed of different types of tissues. For this case, tissue classification using a certain number of pixels in an ROI is superior to that using a single pixel. However, the improvement of tissue classification by the enlargement of an ROI is limited because the classification using a large ROI provides a uniform tissue classification image, whereas the arterial wall is composed of different kinds of tissues. Therefore, there should be

 an optimum size of an ROI. As shown in Fig. 4(a), the recognition rates became maximum in most arteries when the size of an ROI was 1,500 μm × 1,500 μm.
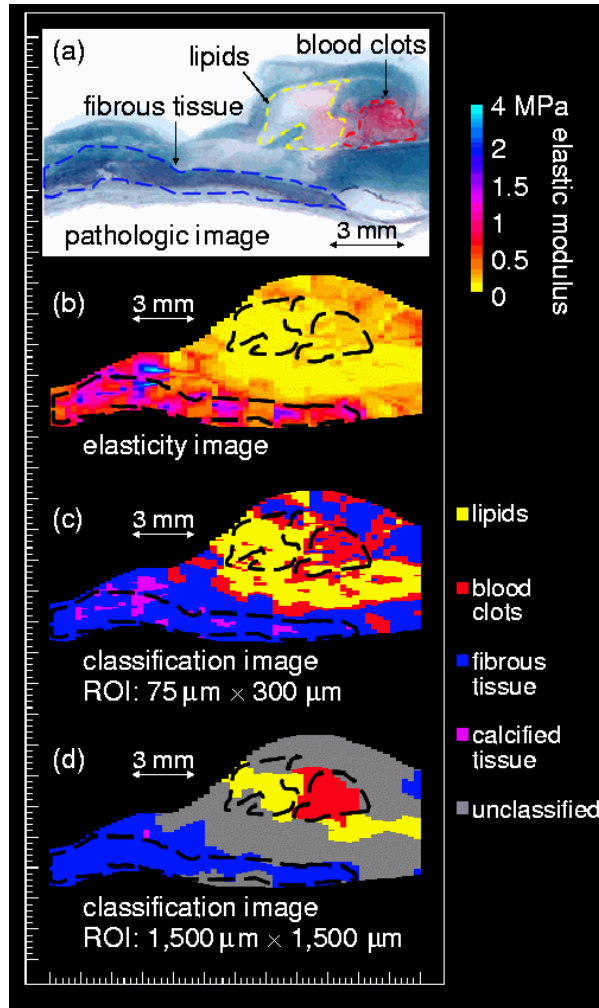

Figure 3. Example of tissue classification. (a) Pathological image of an arterial wall subjected to elastica-Masson staining. (b) Elasticity image. (c) Tissue classification image (ROI size: 1 × 1 pixel). (d) Tissue classification image (ROI size: 5 × 20 pixels).

In this study, the optimum threshold T_o was determined by considering the ratio ($CMR(T_o)$) of the number of correctly classified pixels (the numerator of

eq. (2.3)) to the number of misclassified pixels (the numerator of eq. (2.4)) for all arteries composed of different types of tissues, which was evaluated as follows:

$$\mathrm{CMR}(T_o) = \frac{\sum_i N_{i,\mathrm{all}}}{\sum_i F_{i,\mathrm{all}}},$$

(3.1)

where $N_{i,\mathrm{all}}$ and $F_{i,\mathrm{all}}$ are the sum of correctly classified pixels of tissue i and that of misclassified pixels of tissue i, respectively, for all arteries composed of different types of tissues. Figure 5 shows the relationship between threshold T_o for the likelihood function and the average $\mathrm{CMR}(T_o)$ of all arteries composed of different types of tissues. As shown in Fig. 5, the $\mathrm{CMR}(T_o)$ reached the maximum when the threshold T_o was 0.21.
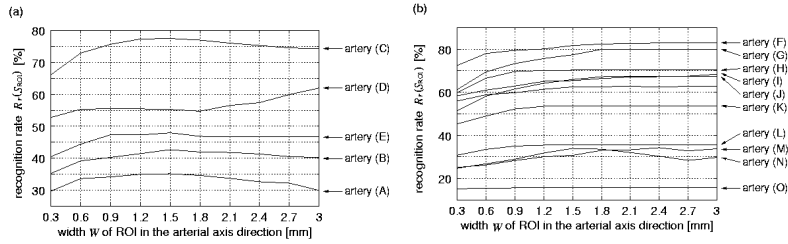

Figure 4. Relationship between width W of an ROI in the longitudinal direction and the recognition rate $R_r(S_{\mathrm{ROI}})$. (a) Arteries composed of several types of tissues. (b) Arteries composed of a single tissue. Each line shows the recognition rate $R_r(S_{\mathrm{ROI}})$ of the corresponding artery.
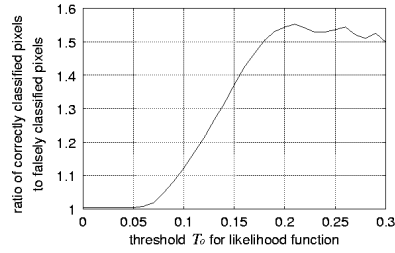

Figure 5. Relationship between threshold T_o for the likelihood function and the ratio of the number of correctly classified pixels to the number of misclassified pixels in all arteries composed of several types of tissues.

4. Conclusions

In this study, tissue classification based on the likelihood function with the configured appropriate ROI size (not a single pixel) and a lower limit of likelihood were investigated. Using the elasticity distribution of an ROI, the

differentiation of lipids from blood clots and that of fibrous tissue from calcified tissue were improved.

References

1. R. T. Lee, A. J. Grodzinsky, E. H. Frank, R. D. Kamm and F. J. Schoen, *Circulation* **83**, 1764 (1991).
2. E. Falk, P. K. Shah and V. Fuster, *Circulation* **92**, 657 (1995).
3. M. J. Davies, *Circulation* **94**, 2013 (1996).
4. J. Golledge, R. M. Greenhalgh and A. H. Davies, *Stroke* **31**, 774 (2000).
5. M. V. McConnell, M. Aikawa, S. E. Maier, P. Ganz, P. Libby and R. T. Lee, *Arterioscler. Thromb. Vasc. Biol.* **19**, 1956 (1999).
6. B. N. Potkin, A. L. Bartorelli, J. M. Gessert, R. F. Neville, Y. Almagor, W. C. Roberts and M. B. Leon, *Circulation* **81**, 1575 (1990).
7. A. P. G. Hoeks, C. J. Ruissen, P. Hick and R. S. Reneman, *Ultrasound Med. Biol.* **11**, 51 (1985).
8. A. P. G. Hoeks, X. Di, P. J. Brands and R. S. Reneman, *Ultrasound Med. Biol.* **19**, 727 (1993).
9. T. Länne, H. Stale, H. Bengtsson, D. Gustafsson, D. Bergqvist, B. Sonesson, H. Lecerof and P. Dahl, *Ultrasound Med. Biol.* **18**, 451 (1992).
10. P. J. Brands, A. P. G. Hoeks, M. C. Rutten and R. S. Reneman, *Ultrasound Med. Biol.* **22**, 895 (1996).
11. D. H. Bergel, *J. Physiol.* **156**, 445 (1961).
12. L. H. Peterson, R. E. Jensen and J. Parnel, *Circ. Res.* **8**, 622 (1960).
13. K. Hayashi, H. Handa, S. Nagasawa, A. Okamura and K. Moritake, *J. Biomech.* **13**, 175 (1980).
14. H. Kanai, M. Sato, Y. Koiwa and N. Chubachi, *IEEE Trans. Ultrason. Ferroelect. Freq. Contr.* **43**, 791 (1996).
15. H. Hasegawa, H. Kanai, Y. Koiwa and N. Chubachi, *Electron. Lett.* **33**, 340 (1997).
16. H. Kanai, H. Hasegawa, M. Ichiki, F. Tezuka and Y. Koiwa, *Circulation* **107**, 3018 (2003).
17. H. Hasegawa and H. Kanai, *IEEE Trans. Ultrason. Ferroelect. Freq. Contr.* **53**, 2050 (2006).
18. H. Hasegawa, H. Kanai, N. Hoshimiya and Y. Koiwa, *J. Med. Ultrason.* **31**, 81 (2004).
19. J. Inagaki, H. Hasegawa, H. Kanai, M. Ichiki and F. Tezuka, *Jpn. J. Appl. Phys.* **44**, 4593 (2005).
20. J. Inagaki, H. Hasegawa, H. Kanai, M. Ichiki and F. Tezuka, *Jpn. J. Appl. Phys.* **45**, 4732 (2006).
21. K. Tsuzuki, H. Hasegawa, H. Kanai, M. Ichiki and F. Tezuka, *Ultrasound Med. Biol.* **34**, 573 (2008).

22. K. Tsuzuki, H. Hasegawa, H. Kanai, M. Ichiki and F. Tezuka, *Jpn. J. Appl. Phys.* **47**, 4180 (2008).